Generation of whistler waves by continuous HF heating of the upper ionosphere

A. Vartanyan[1], G. M. Milikh[1], B. Eliasson[1,2], A. C. Najmi[1], C. L. Chang[3], M. Parrot[4], and K. Papadopoulos[1,3]

[1]Department of Physics and Astronomy, University of Maryland, College Park, MD, USA
[2]Department of Physics, University of Strathclyde, Glasgow, UK
[3]Technology Solutions, BAE Systems, Arlington, VA, USA
[4]Laboratoire de Physique et Chimie de l'Environnement et de l'Espace, CNRS, Orleans, France

Abstract

Broadband whistler waves in the frequency range 7-10 kHz and 15-19 kHz, generated by F-region CW HF ionospheric heating in the absence of electrojet currents, were detected by the DEMETER satellite overflying the HAARP transmitter during previous HAARP/BRIOCHE campaigns. The whistler waves are in a frequency range corresponding to the F-region Lower-Hybrid (LH) frequency and its harmonic - generated by mode conversion of LH waves that were parametrically excited by HF-pump-plasma interaction at the upper hybrid layer. The letter discusses the basic physics and presents a model that conjectures: (i) The whistler wave observed at the LH frequency is due to the interaction of the LH waves with meter-scale field aligned striations; (ii) The whistler wave at twice the LH frequency is due to the interaction of two counter-propagating LH waves. The model is supported by numerical simulations that show good agreement with the observations.

1 Introduction

The generation of electromagnetic waves in the ELF/VLF frequency range by modulated HF heating of the ionospheric plasma has been the subject of many studies. Experiments and theory revealed that two completely different physical processes control their generation: (1) electrojet current modulation, which relies on modulated HF heating of the D/E region plasma electrons in the presence of electrojet currents and creates the Polar ElectroJet (PEJ) antenna, capable of VLF generation up to 10-20 kHz [Rietveld et al., 1986; Papadopoulos and Chang, 1985; Cohen et al., 2011]; (2) Ionospheric Current Drive (ICD) [Papadopoulos et al., 2011b,a], which relies on modulated heating of the electron pressure in the F region, is independent of the presence of electrojet currents and capable of ELF generation up to 60 Hz.

The objective here will be to present observations indicative of a third mechanism that injects broadband ($\Delta f/f \approx 0.1$ - 0.25) whistler waves into the magnetosphere. Whistler waves in the frequency range 7-10 kHz and 15-19 kHz, generated by F region CW HF ionospheric heating in the absence of electrojet currents, were detected by the DEMETER satellite overflying the HAARP transmitter during HAARP/BRIOCHE campaigns. The whistler waves are in a frequency range corresponding to the F region Lower-Hybrid (LH) frequency and its harmonic, believed to be generated by mode conversion of LH waves that were parametrically excited by HF-pump-plasma interactions at the upper hybrid layer. We will discuss the basic physics and presents a model that

conjectures: (i) The whistler wave observed at the LH frequency is due to the interaction of the LH waves with meter-scale field aligned striations; (ii) The whistler wave at twice the LH frequency is due to the interaction of two counter-propagating LH waves. The model is supported by numerical simulations and will be shown to be in good agreement with the observations.

2 Experimental Observations

We report below the results of two day-time HAARP/BRIOCHE experiments conducted during flyovers of the DEMETER satellite, during which HAARP operated in O-mode at its maximum 3.6 MW, pointed along the MZ. DEMETER travels along its circular polar orbit at a speed of about 7.5 km/s and altitude 670 km. The experiments were diagnosed by the DEMETER Instrument Champ Electrique (ICE) , that measured one component of the electric field in the VLF range at a sampling rate of 40 kHz, and the Instrument Sonde de Langmuir (ISL) , that measured the electron density at a sampling rate of 1 Hz. Ground diagnostics included Stimulated Electromagnetic Emission (SEE) observations, the on-site ionosonde and magnetometer, and the Kodiak coherent radar located approximately 650 km from HAARP. Ionograms were used to select the heating frequency - chosen to either match the critical frequency (f_0F_2) or the third electron gyro-harmonic (4.35 MHz). Key parameters of the experiments are given in Table 1. The major difference between the two experiments (other than HF frequency) was CW heating for Exp. 1, and 0.7 Hz square pulse modulation heating for Exp. 2. During the experiments the F region was smooth, with weak-to-

Experiment label	Heating time (UT)	f_H (MHz) / h_r (km)	f_0F_2 (MHz) / h_mF_2 (km)	ΔR (km) / L_{EW} (km)	HF heating regime
1	10/16/2009 20:15-20:45	5.1 / 220	5.15 / 225	69 / 32	CW
2	02/10/2010 20:15-20:34	4.25 / 200	5.5 / 230	40 / 39	Modulated at 0.7 Hz

Table 1: Key experimental information, including the HF frequency (f_H) and reflection height (h_r), the critical frequency (f_0F_2) and critical height (h_mF_2), the closest approach of DEMETER to the HAARP MZ (ΔR) and the E-W half-power beam width at the heating altitude (L_{EW}), and the HF heating settings.

moderate D/E region absorption. Kodiak radar measurements (not shown) during Exp. 1 show strong reflections during heating, indicating the build-up of strong plasma striations; Kodiak radar was unavailable during Exp. 2.

The experimental results are shown in Figures 1 and 2. Figures 1a and 1b show spectrograms observed by ICE during DEMETER flyovers of HAARP at the time of the experiments, with time measured relative to the closest approach of the MZ. The spectrograms were computed directly from the ICE waveform data using a short-time Fourier transform. In both figures whistler signals are observed in the vicinity of the MZ over approximately 10 s, corresponding to a distance of 75 km [1]. Note that the regular temporal structure of the whistler waves in Figure 1b is attributable to the 0.7 sec on-off square pulse HF heating, while the irregular structure in Figure 1a can be

[1] We should remark that the spectrograms contain features that are not related to our experiments: a faint band at $\sim$ 7 - 8 kHz stretching across the entire time domain, corresponding to naturally occurring LH oscillations; broadband and temporally narrow spectral features outside of the heated region due to short timescale transient processes, such as whistler waves created by lightning; strong but quite narrowband signals (e.g. at 16.5 and 18.5 kHz) due to man-made transmissions.

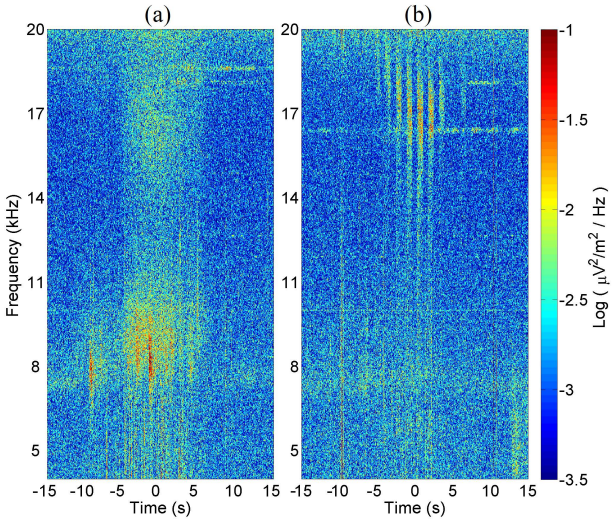

Figure 1: Spectrogram seen by DEMETER during Experiment 1 on 10/16/09 in which HAARP used CW heating (a), and during Experiment 2 on 02/10/10 (b) in which HAARP used 0.7 Hz square pulse modulated heating. In both cases time = 0 corresponds to the closest approach of DEMETER to the HAARP MZ.

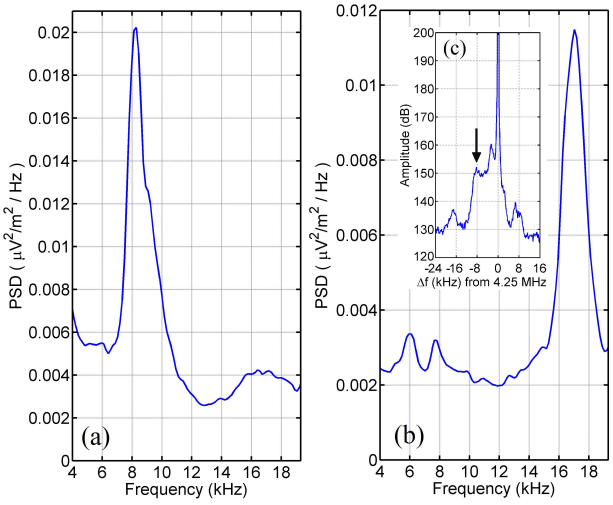

Figure 2: Power spectral density versus frequency measured on 10/16/09 (a) and on 02/10/10 (b), obtained from a 2 s average of the Figure 1 observations near the closest approach of the MZ.

attributed to whistler wave focusing by artificial ducts due to the HF heating [Woodroffe et al., 2013].

Figures 2a,b show the power spectral density (PSD) estimates for the two experiments, measured near the closest approach to the HAARP MZ. For Exp. 1 (Figure 2a) the central frequencies are at 8.2 kHz and 16.5 kHz, corresponding to the F region LH frequency and its harmonic, with Full Width at Half Maximum (FWHM) of approximately 2 kHz and 3 kHz. For Exp. 2 (Figure 2b) the central frequency is near 16.8 kHz, close to the LH harmonic, and has a 2 kHz FWHM. Note that the peak near 8 kHz in Figure 2b is of natural origin, as mentioned above. In addition to the standard diagnostics, SEE measurements were available during Exp. 2, as shown by the inserted Figure 2c. The large central peak at $\delta f = 0$ is the backscattered pump wave; the smaller peak marked by the arrow (shifted down by 8.5 kHz) is the so-called Downshifted Maximum (DM), whose relevance will become clear below.

3 Discussion and Theoretical Considerations

The observed whistler waves are in a frequency range corresponding to the F-region LH frequency and its second harmonic. In this section we motivate that the observations are due to mode conversion of LH waves to whistler waves, where the LH waves were parametrically excited by the HF pump interacting with the plasma at the upper hybrid layer. Moreover, in examining the observations presented in Figures 1 and 2 we find a major peculiarity: while in Exp. 1 whistler waves were measured at the LH frequency and its second harmonic, in Exp. 2 whistler waves appeared only at the harmonic of the LH. To understand this puzzling absence and subsequent theoretical discussions, it pays to first review the HF pump wave-plasma interaction happening in the heated region.

3.1 Parametric Excitation of LH Waves at the UH Resonance

As an O-mode HF wave of frequency f_0 is transmitted along the MZ, it propagates to the reflection point where $f_0 = f_{pe}$, the plasma frequency. Along the way, it additionally encounters the Upper Hybrid (UH) Resonance (UHR) $f_0^2 = f_{pe}^2 + f_{ce}^2$, where f_{ce} is the electron gyrofrequency.

At the UHR, the HF pump wave mode converts to UH waves on natural or self-focusing driven irregularities , trapping and amplifying the UH waves until parametric instabilities are triggered [Gurevich, 2007] that excite other wave modes. One such wave mode, the LH wave, is manifested by the DM in the SEE spectrum and has been confirmed by numerous SEE observations. Several theoretical models have been proposed for DM generation, culminating in "cascade" models that naturally explain the multiple DM features (2DM, 3DM, $\cdots$) that are regularly observed during SEE experiments. The significance of this is that the presence of a DM is a proxy of parametrically excited LH waves, as is the case for Exp. 2. In fact, the DM feature in Figure 2c is downshifted by about 8.5 kHz, while a second smaller peak is downshifted by 17 kHz (2DM).

3.2 Striation Development and the Missing LH Peak

Several theoretical and experimental studies [Bell and Ngo, 1990; Eliasson and Papadopoulos, 2008; Shao et al., 2012; Vaskov et al., 1998] have shown that LH waves can be converted into whistler waves (W) (and vice versa) in the presence of static meter-scale plasma density striations (D):

$$LH(f_l, \pm k_l) + D(0, \mp k_{str}) \rightarrow W(f_l, 0)$$

Following the start of HF heating, the development of SEE-related striations and the DM (and hence LH waves) has been shown to be less than 20 ms [Sergeev et al., 2013], while the development of significant meter-scale sized striations take much longer, on the order of 5-10 s [Honary et al., 2011]. These times scales can be demonstrated by an experiment we conducted at HAARP, with conditions similar to those in Exp. 2 (daytime, quiet ionosphere, $f_H = 5.75$ MHz $\approx 4f_{ce}$, h_r = 200 km, pulsed MZ heating). SEE measurements and GPS Slant Total Electron Content (STEC) data were simultaneously collected. The result are presented in Figure 3 and show SEE with a well-developed DM and simultaneously an increase in STEC, corresponding to the formation of plasma density striations [Milikh et al., 2008]. The STEC had a build-up time of about 5-10 s (Figure 3a), while the buildup time of the DM was under 20 ms (Figure 3b), and became fully developed with multiple DM features after about 10 s (Figure 3c). These differences in time-scales explain the missing peak near the LH frequency in Figure 2b. Recall that Exp. 1 used CW heating, while Exp. 2 used pulsed heating with on/off times of 0.7 s. Figure 3a,b illustrates that using short heating pulses with 0.7 s on and 0.7 s off, such as in Exp. 2, is enough to generate LH waves, but does not allow for the development of significant artificial striations. Without a sufficient build-up of striations, the

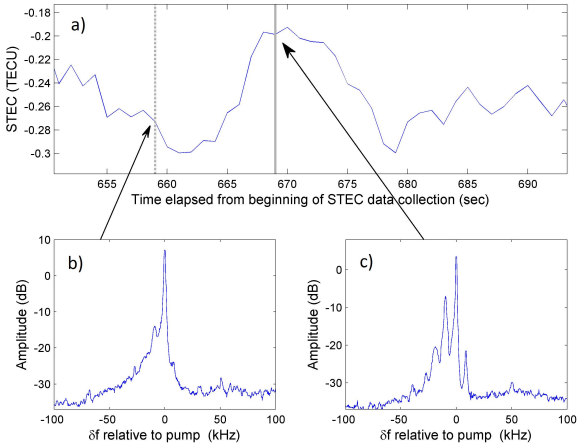

Figure 3: Measurements of STEC during an HF heating experiment (a); variation in STEC has a timescale of several seconds. Simultaneously, SEE was measured 20 ms after the start of heating (b), already showing signs of DM. SEE after 10 s of heating shows well developed DM, along with 2DM and 3DM (c).

linear mode conversion mechanism would be too inefficient to be observed by DEMETER, which is consistent with the absence of VLF near the LH frequency in Figure 2b.

3.3 Whistler Waves at the LH Harmonic

The main peak in Figure 2a near the LH frequency is naturally explained by the fact that CW heating generates meter-scale striations necessary for LH-whistler conversion. Our attention now shifts to the LH second harmonic in Figure 2a,b. LH waves with a frequency near (or greater than) twice the LH frequency cannot exist, since this would break the LH existence requirement $\pi/2-\theta < \sqrt{m_e/m_i}$, where θ is the angle between the LH wave vector and the background geomagnetic field, $\boldsymbol{B}_0$. Thus the second harmonic must be generated from a different kind of interaction. We suggest that the mechanism responsible for whistlers at the LH harmonic is due to the nonlinear interaction of oppositely propagating LH waves, analogous to counter-streaming Langmuir waves interacting to give EM waves with twice the Langmuir frequency [Akimoto et al., 1988]:

$$LH(f_l, +k_l) + LH(f_l, -k_l) \rightarrow W(2f_l, 0) \tag{1}$$

Such a mechanism does not directly rely on striations, but instead relies on the density fluctuations due to the large amplitude LH electric field.

3.4 LH-whistler Mode Conversion: Model and Simulations

Eliasson and Papadopoulos [2008] studied LH-whistler mode conversion in the presence of plasma density striations by formulating the problem into two coupled equations, corresponding to the whistler and LH wave. The whistler wave was shown to be governed by the evolution equation for the whistler particle current ($\boldsymbol{j}_W$)

$$\frac{\partial \boldsymbol{j}_W}{\partial t} = -\frac{e\lambda_e^2}{m_e}(1-\lambda_e^2\nabla^2)^{-1}\boldsymbol{\nabla}\times\left[\boldsymbol{\nabla}\times((n_{str}+n_{LH})\boldsymbol{E}_{LH}+\boldsymbol{j}_W\times\boldsymbol{B}_0)\right], \tag{2}$$

while the LH particle current ($\boldsymbol{j}_{LH}$) is governed by

$$\frac{\partial \boldsymbol{j}_{LH}}{\partial t} = \nabla^{-2}\left\{\frac{e}{m_e}\boldsymbol{\nabla}\times[\boldsymbol{\nabla}\times(n_{str}\boldsymbol{E}_W+\boldsymbol{j}_{LH}\times\boldsymbol{B}_0)] - \frac{e}{m_i}\boldsymbol{\nabla}\left[\boldsymbol{\nabla}\cdot(\boldsymbol{j}_{LH}\times\boldsymbol{B}_0)\right]\right\}. \tag{3}$$

The particle currents $\boldsymbol{j}_W$ and $\boldsymbol{j}_{LH}$ are define as the product of electron number density and velocity, while the whistler and LH electric fields are given by [Eliasson and Papadopoulos, 2008]

$$\boldsymbol{E}_W = -(\boldsymbol{j}_W\times\boldsymbol{B}_0)/n_0 \tag{4}$$

$$\boldsymbol{E}_{LH} = -\boldsymbol{\nabla}\left[\nabla^{-2}\left[\boldsymbol{\nabla}\cdot(\boldsymbol{j}_{LH}\times\boldsymbol{B}_0)\right]/n_0\right], \tag{5}$$

where $\lambda_e = c/\omega_{pe}$ is the electron inertial length, $\boldsymbol{B}_0$ is the background field vector, n_0 is a constant background plasma density and n_{str} accounts for external density striations. Thus in the presence of density striations the LH electric field can drive whistler waves, and vice versa. Note that n_{LH}, which is the density fluctuation of the LH wave, was neglected in Eliasson and Papadopoulos [2008] during linearization of the equations. We generalized the model by keeping this nonlinear coupling, for reasons that will become clear below. The density fluctuations are obtained from the continuity equation

$$\frac{\partial n_{LH}}{\partial t} + \boldsymbol{\nabla}\cdot\boldsymbol{j}_{LH} = 0. \tag{6}$$

Eliasson and Papadopoulos [2008] showed that efficient resonant mode conversion from LH to whistler waves occurs when the striation full-width (D_{str}) is comparable to half the perpendicular wavelength of the LH wave:

$$D_{str} \sim \frac{\pi}{k_{l,\perp}}. \tag{7}$$

During this resonant mode conversion process the LH and whistler waves have the same frequency, $\omega_l = \omega_w = \omega$; the wave vector components along the geomagnetic field are the same for the LH and whistler wave $k_{l,\parallel} = k_{w,\parallel} = k_\parallel$, but their perpendicular components $k_{l,\perp}$ and $k_{w,\perp}$ can be different. While the LH wave propagates almost perpendicular to the magnetic field, the whistler wave propagates primarily along the magnetic field but can be slightly oblique. With these conditions the LH and whistler dispersion relations give

$$\omega_l^2 = \omega^2 = \frac{\omega_{l,0}^2 k_{l,\perp}^2 + \omega_{ce}^2 k_\parallel^2}{k_{l,\perp}^2 + k_\parallel^2} \approx \frac{\omega_{l,0}^2 k_{l,\perp}^2 + \omega_{ce}^2 k_\parallel^2}{k_{l,\perp}^2} \tag{8}$$

$$\omega_w^2 = \omega^2 = \lambda_e^4 k_\parallel^2 (k_{w,\perp}^2 + k_\parallel^2)\omega_{ce}^2 \approx \lambda_e^4 k_\parallel^4 \omega_{ce}^2 \tag{9}$$

where $\omega_{l,0} = 2\pi f_{l,0} = \sqrt{\omega_{ce}\omega_{ci}}$ is the LH oscillation frequency, and parallel whistler propagation was assumed ($k_{w,\perp} = 0$). Eliminating $k_\parallel^2$ in Equation (8) by using Equation (9), we then obtain

$$k_{l,\perp}^2 = \frac{\omega_{ce}\omega}{\lambda_e^2(\omega^2 - \omega_{l,0}^2)} = \frac{\sqrt{m_i/m_e}(f/f_{l,0})}{\lambda_e^2\left[(f/f_{l,0})^2 - 1\right]} \tag{10}$$

By using the 2007 International Reference Ionosphere (IRI), we can estimate the local plasma parameters necessary for finding $k_{l,\perp}$ from Equation (10). We take the electron gyrofrequency to be $f_{ce} = 1.45$ MHz near altitudes of 200-220 km at HAARP. For typical ionospheric conditions, such as in Exp. 1 and 2, the IRI model gives $f_{l,0} \approx 7.5$ kHz, $\lambda_e \approx 9$ m. If we take $f = 8.2$ kHz, corresponding to the main peak in Figure 2a, then Equation (10) gives an approximate range of $k_{l,\perp} \approx$ 3-4 m^{-1} for the relevant altitudes. The corresponding resonant striation width can be found from Equation (7) to be $D_{str} \approx 1$ m, which is the characteristic size of small scale striations known to exist during continuous HF heating [Carpenter, 1974].

Consider the model (2) - (6) with input parameters similar to the above estimates. We take $n_0 = 3.1 \times 10^5$ cm^{-3} and assume a Gaussian depletion profile for n_{str} with a full-width $D_{str} =$ 0.8 m and depletion amplitude that is 1.25% of n_0. Moreover, the initial conditions are set to be three LH wave packets directly on top of the striation, all with $k_{l,\perp} = 4$ m^{-1}. For the first wave packet, the angle (of the wave fronts) relative to $\boldsymbol{B}_0$ is set to resonantly generate whistler waves at the LH frequency by (linearly) interacting with the striation [Eliasson and Papadopoulos, 2008]. For the remaining two wave packets: one is set to be exactly perpendicular ($\theta = \pi/2$), while the angle of the other is (analogously) set to resonantly generate whistler waves at the LH harmonic by nonlinearly interacting with the perpendicular LH wave packet. Running a simulation with this setup generates mode-converted whistler waves with frequencies that correspond to the LH frequency and its harmonic, as shown in Figure 4. Figure 4a reveals the magnitude of the LH electric field vector, while Figure 4b shows the magnitude of the whistler magnetic field vector. The spectrum of the whistler magnetic field, as seen from a stationary observation point at the top of the simulation domain ($z = 9$ km), is plotted in Figure 4c and shows good agreement with the experimentally observed PSD in Figure 2a. The vertical lines indicate the LH frequency and its harmonic, and as expected they are close to the peaks of the whistler spectrum. If the striation amplitude were to be set to zero in the simulation, then only whistler genera-

tion at the LH harmonic would result, thus confirming the whistler spectrum observed Figure 2b.

4 Conclusions

This letter described two HAARP/DEMETER experiments in which VLF waves of artificial origin were detected by the DEMETER satellite while overflying the HF-heated region of the ionosphere. The observations were shown to be consistent with parametrically excited LH waves being mode converted to whistler waves during HF heating. The VLF near the LH frequency observed during Exp. 1, in which we have used CW HF heating, was shown to be due to resonant mode conversion to whistler waves in the presence of artificially pumped meter-scale striations. The VLF near the LH harmonic observed during both Exp. 1 and Exp. 2 was shown to be generated by a different mechanism: due to the nonlinear 3-wave interaction of two counter propagating LH waves generating a whistler wave. Simulation results based on the generalized LH-whistler mode conversion model of Eliasson and Papadopoulos [2008] were presented, where a nonlinear coupling term was added to the model. The results of the simulation showed mode-converted whistlers with frequencies near the LH frequency and its harmonic, consistent with the observed spectrum during Exp. 1. It was also shown that the absence of any VLF features near the LH frequency during Exp. 2 was due to the fact that Exp. 2 used short heating pulses, thus not allowing the development of significant meter-scale striations and preventing an efficient linear coupling from LH waves to whistlers. The nonlinear coupling, however, does not directly rely on striations. which is consistent with the whistler spectrum observed during Exp. 2.

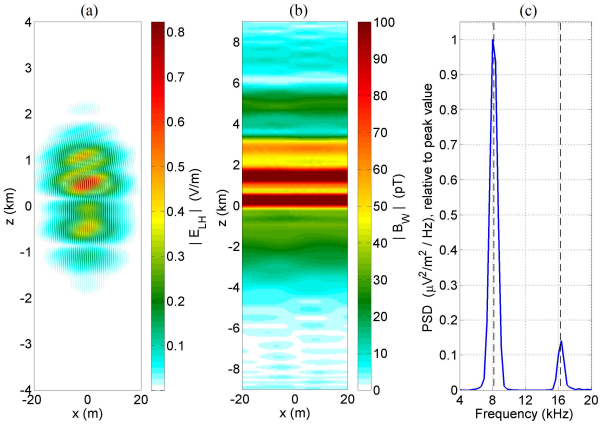

Figure 4: Simulation results showing generation of mode-converted whistler waves with frequencies at the LH frequency and its second harmonic: (a) The magnitude of the LH electric field in V/m, (b) magnitude of the whistler magnetic field in pT, and (c) spectrum of the y-component whistler electric field, relative to the peak value; the vertical lines in (c) represent the LH frequency and its second harmonic.

Acknowledgements. AV and GM were supported by DARPA via a subcontract N684228 with BAE Systems and also by the MURI grant FA95501410019. We are very thankful to Paul Bernhardt, Stan Briczinski and Carl Siefring for sharing their SEE data. We acknowledge CNES for the use of the DEMETER data. We acknowledge very useful discussions with Andrei Demekhov and Lena Titova, and Mike McCarrick's expert help in conducting the HAARP experiments.

References

Akimoto, K., Rowland, H. L., and Papadopoulos, K. (1988). Electromagnetic radiation from strong langmuir turbulence. *Physics of Fluids*, 31(8):2185–2189.

Bell, T. F. and Ngo, H. D. (1990). Electrostatic Lower Hybrid Waves Excited by Electromagnetic

Whistler Mode Waves Scattering From Planar Magnetic-Field-Aligned Plasma Density Irregularities. *J. Geophys. Res.*, 95(A1):149–172.

Carpenter, G. B. (1974). VHF and UHF bistatic observations of a region of the ionosphere modified by a high power radio transmitter. *Radio Sci.*, 9(11):965–969.

Cohen, M. B., Inan, U. S., Piddyachiy, D., Lehtinen, N. G., and Gokowski, M. (2011). Magnetospheric injection of ELF/VLF waves with modulated or steered HF heating of the lower ionosphere. *J. Geophys. Res.*, 116(A06308).

Eliasson, B. and Papadopoulos, K. (2008). Numerical study of mode conversion between lower hybrid and whistler waves on short-scale density striations. *J. Geophys. Res.*, 113(A09315).

Gurevich, A. V. (2007). Nonlinear effects in the ionosphere. *Phys. - Uspekhi*, 50(11):1091 – 1121.

Honary, F., Borisov, N., Beharrell, M., and Senior, A. (2011). Temporal development of the magnetic zenith effect. *J. Geophys. Res.*, 116(A06309).

Milikh, G., Gurevich, A., Zybin, K., and Secan, J. (2008). Perturbations of GPS signals by the ionospheric irregularities generated due to HF-heating at triple of electron gyrofrequency. *Geophys. Res. Lett.*, 35(L22102).

Papadopoulos, K. and Chang, C. L. (1985). GENERATION OF ELF/ULF WAVES IN THE IONOSPHERE BY DYNAMO PROCESSES. *Geophys. Res. Lett.*, 12(5):279–282.

Papadopoulos, K., Chang, C. L., Labenski, J., and Wallace, T. (2011a). First demonstration of HF-driven ionospheric currents. *Geophys. Res. Lett.*, 38(L20107).

Papadopoulos, K., Gumerov, N. A., Shao, X., Doxas, I., and Chang, C. L. (2011b). HF-driven currents in the polar ionosphere. *Geophys. Res. Lett.*, 38(L12103).

Rietveld, M. T., Kopka, H., and Stubbe, P. (1986). D-region characteristics deduced from pulsed ionospheric heating under aurora1 electrojet conditions. *J. Atmos. Terr. Phys.*, 48(4):311–326.

Sergeev, E., Grach, S., Shindin, a., Mishin, E., Bernhardt, P., Briczinski, S., Isham, B., Broughton, M., LaBelle, J., and Watkins, B. (2013). Artificial Ionospheric Layers during Pump Frequency Stepping Near the 4th Gyroharmonic at HAARP. *Phys. Rev. Lett.*, 110(6):065002.

Shao, X., Eliasson, B., Sharma, A. S., Milikh, G., and Papadopoulos, K. (2012). Attenuation of whistler waves through conversion to lower hybrid waves in the low-altitude ionosphere. *J. Geophys. Res.*, 117(A04311).

Vaskov, V. V., Budko, N. I., Kapustina, O. V., Mikhailov, Y. M., Ryabova, N. A., Gdalevich, G. L., Komrakov, G. P., and Maresov, A. N. (1998). Detection on the Intercosmos-24 satellite of VLF and ELF waves stimulated in the topside ionosphere by the heating facility 'Sura'. *J. Atmos. Solar-Terrestrial Phys.*, 60(12):1261–1274.

Woodroffe, J. R., Streltsov, A. V., Vartanyan, A., and Milikh, G. M. (2013). Whistler propagation in ionospheric density ducts: Simulations and DEMETER observations. *J. Geophys. Res. Sp. Phys.*, 118(11):7011–7018.